

### Supplementary information:

#### Mechanisms and effects of gas intercalation into ionic liquids confined within charged nanoscale volumes

Fikret Aydin<sup>1</sup>, Alex Abelson<sup>2</sup>, Stephen E. Weitzner<sup>1</sup>, Francesco Fornasiero<sup>1</sup>, Tuan Anh Pham<sup>1</sup>, Eric R. Meshot<sup>2</sup>, and Steven F. Buchsbaum<sup>2\*</sup>

<sup>1</sup>Physical and Life Sciences, Lawrence Livermore National Laboratory, Livermore, CA 94550, USA

<sup>2</sup>Engineering, Lawrence Livermore National Laboratory, Livermore, CA 94550, USA

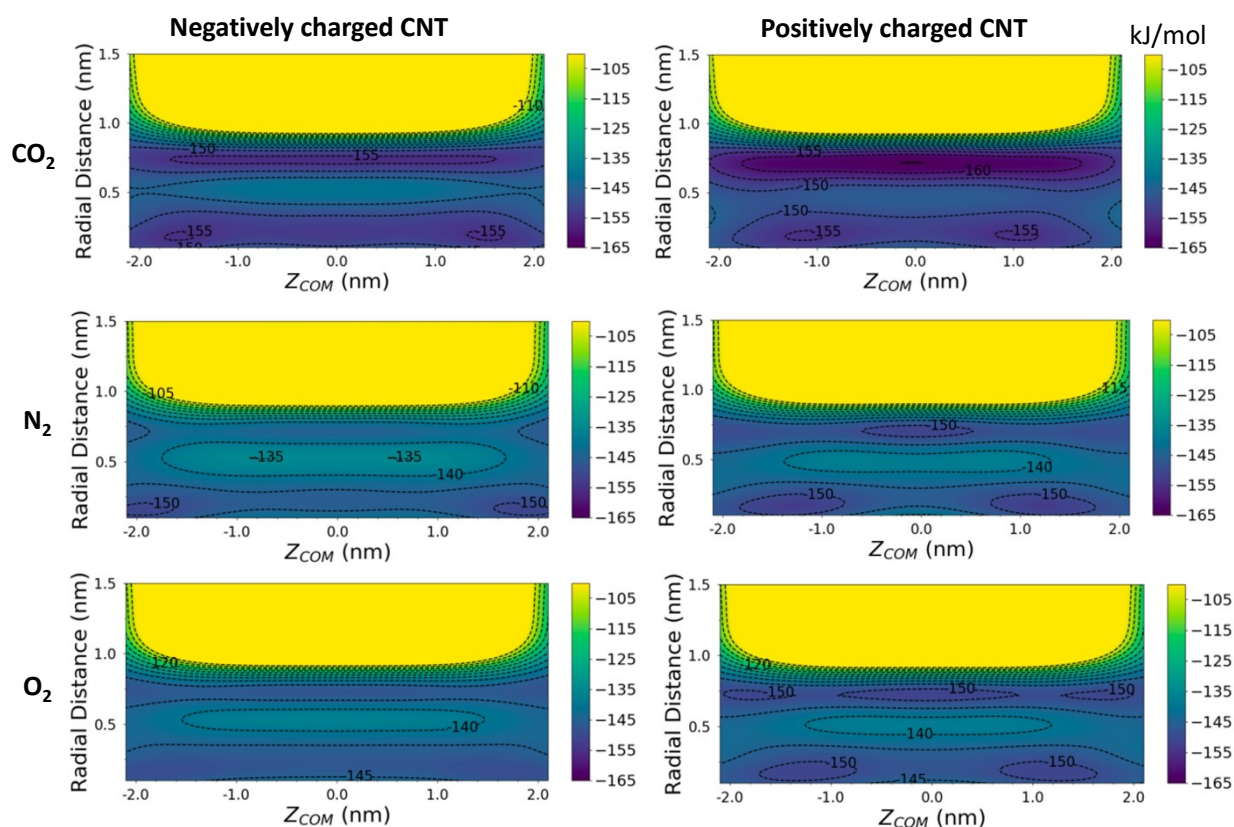


**Figure S1** Two-dimensional potential of mean force (in kJ/mol) of gas molecules transporting through a (A) negatively and (B) positively charged CNT.  $Z_{COM}$  and radial distance indicate the center-of-mass (COM) distances between a gas molecule and the CNT along the CNT axis and radial to the pore axis, respectively.

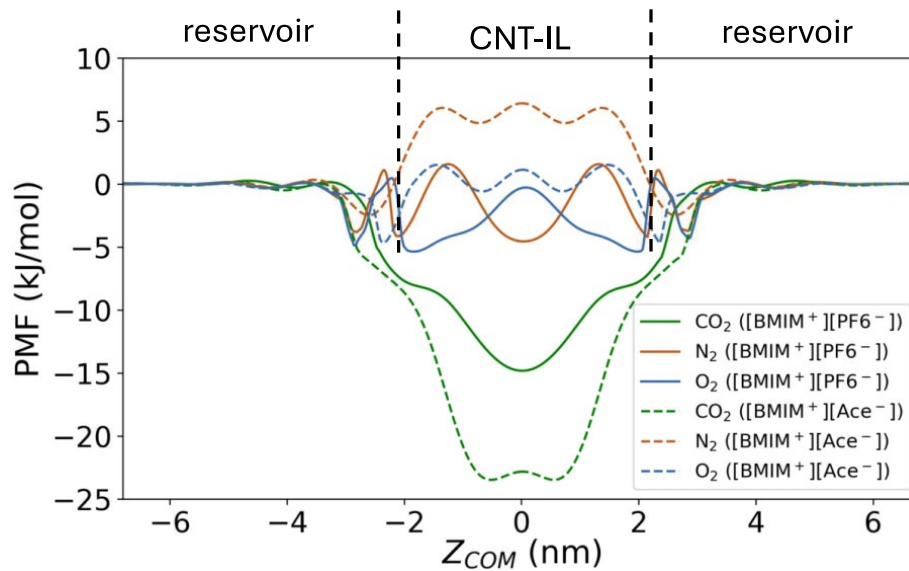


**Figure S2** Comparison of one-dimensional potential of mean forces (PMFs) of different gas molecules transporting through a CNT filled with [BMIM<sup>+</sup>][PF<sub>6</sub><sup>-</sup>] and [BMIM<sup>+</sup>][Ace<sup>-</sup>].

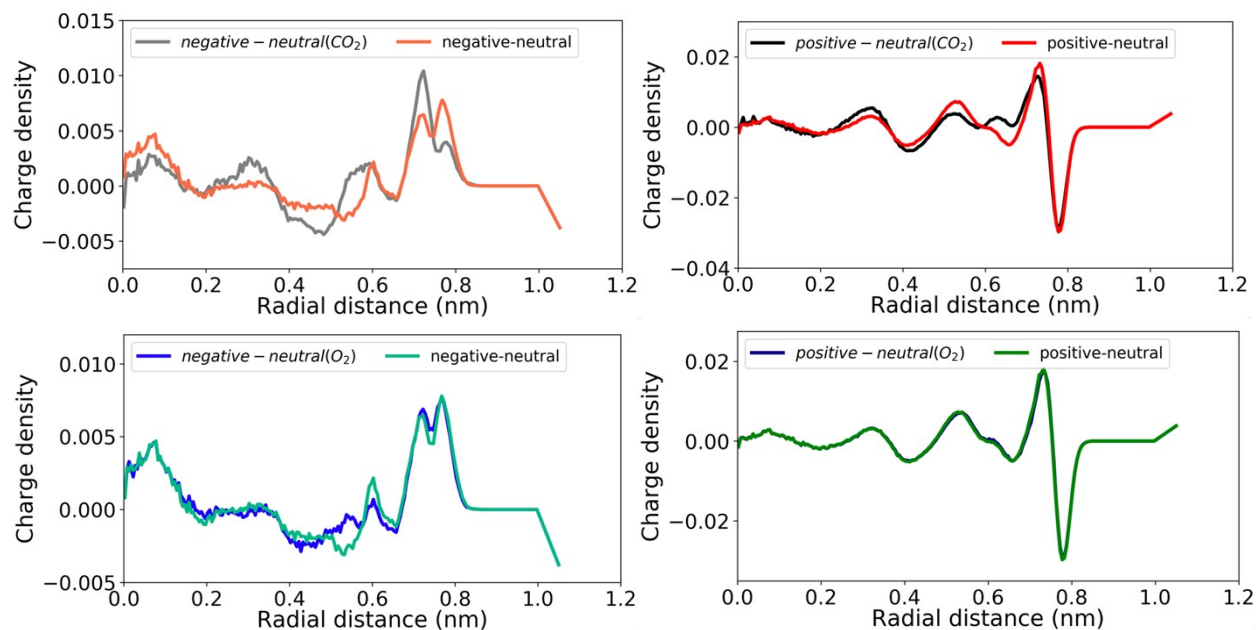


**Figure S3** Effect of CO<sub>2</sub> (top) and O<sub>2</sub> (bottom) uptake on the charge density distributions for the negatively and positively charged CNTs filled with [BMIM<sup>+</sup>][Ace<sup>-</sup>]. The charge density distribution for the neutral CNT was subtracted from the charge density distribution of each charged CNT.

### Discussion simulation results using [BMIM<sup>+</sup>][Ace<sup>-</sup>]

One important aspect of gas separation with CNT-IL systems is the type of IL, which is shown to influence selectivity of gas molecules.<sup>1</sup> To provide groundwork which may inform future studies, we compared energetics of CO<sub>2</sub>, N<sub>2</sub> and O<sub>2</sub> transport through a neutral CNT filled with [BMIM<sup>+</sup>][Ace<sup>-</sup>] (for comparison with Figure 4 of the main text). Force fields for the IL were taken from Mondal et al.<sup>2</sup> 1D PMFs for [BMIM<sup>+</sup>][PF<sub>6</sub><sup>-</sup>] and [BMIM<sup>+</sup>][Ace<sup>-</sup>] show consistent trends for CO<sub>2</sub> (e.g., it is energetically the most favorable gas molecule to intercalate in CNT). On the other hand, there are significant differences in intercalation energies of CO<sub>2</sub>, N<sub>2</sub> and O<sub>2</sub> between [BMIM<sup>+</sup>][PF<sub>6</sub><sup>-</sup>] and [BMIM<sup>+</sup>][Ace<sup>-</sup>]. Specifically, intercalation energies of CO<sub>2</sub>, N<sub>2</sub> and O<sub>2</sub> in [BMIM<sup>+</sup>][Ace<sup>-</sup>] are more clearly separated, which may indicate that [BMIM<sup>+</sup>][Ace<sup>-</sup>] provides a better selectivity among these gas molecules. For example, the free energy difference between intercalations of CO<sub>2</sub> and N<sub>2</sub> is ~11 kJ/mol and ~28 kJ/mol for [BMIM<sup>+</sup>][PF<sub>6</sub><sup>-</sup>] and [BMIM<sup>+</sup>][Ace<sup>-</sup>], respectively. Similarly, the free energy difference between intercalations of CO<sub>2</sub> and O<sub>2</sub> is ~14 kJ/mol and ~23 kJ/mol for [BMIM<sup>+</sup>][PF<sub>6</sub><sup>-</sup>] and [BMIM<sup>+</sup>][Ace<sup>-</sup>], respectively. Similar to charge density calculations done for [BMIM<sup>+</sup>][PF<sub>6</sub><sup>-</sup>], the effect of CNT charge state on the charge density distribution was investigated. CNTs were filled with [BMIM<sup>+</sup>][Ace<sup>-</sup>] and two gas molecules (CO<sub>2</sub> and O<sub>2</sub>) and simulations were performed at various conditions (neutral, negatively, or positively charged CNTs). The results for [BMIM<sup>+</sup>][Ace<sup>-</sup>] are consistent with the previous results for [BMIM<sup>+</sup>][PF<sub>6</sub><sup>-</sup>] (Figure 4), showing that CO<sub>2</sub> uptake has a larger effect on the charge density distribution than O<sub>2</sub>. As mentioned in the main text, we were unable to provide any validation of these results experimentally due to what we believe is a chemical reactivity between tested gases as this IL.<sup>3</sup>

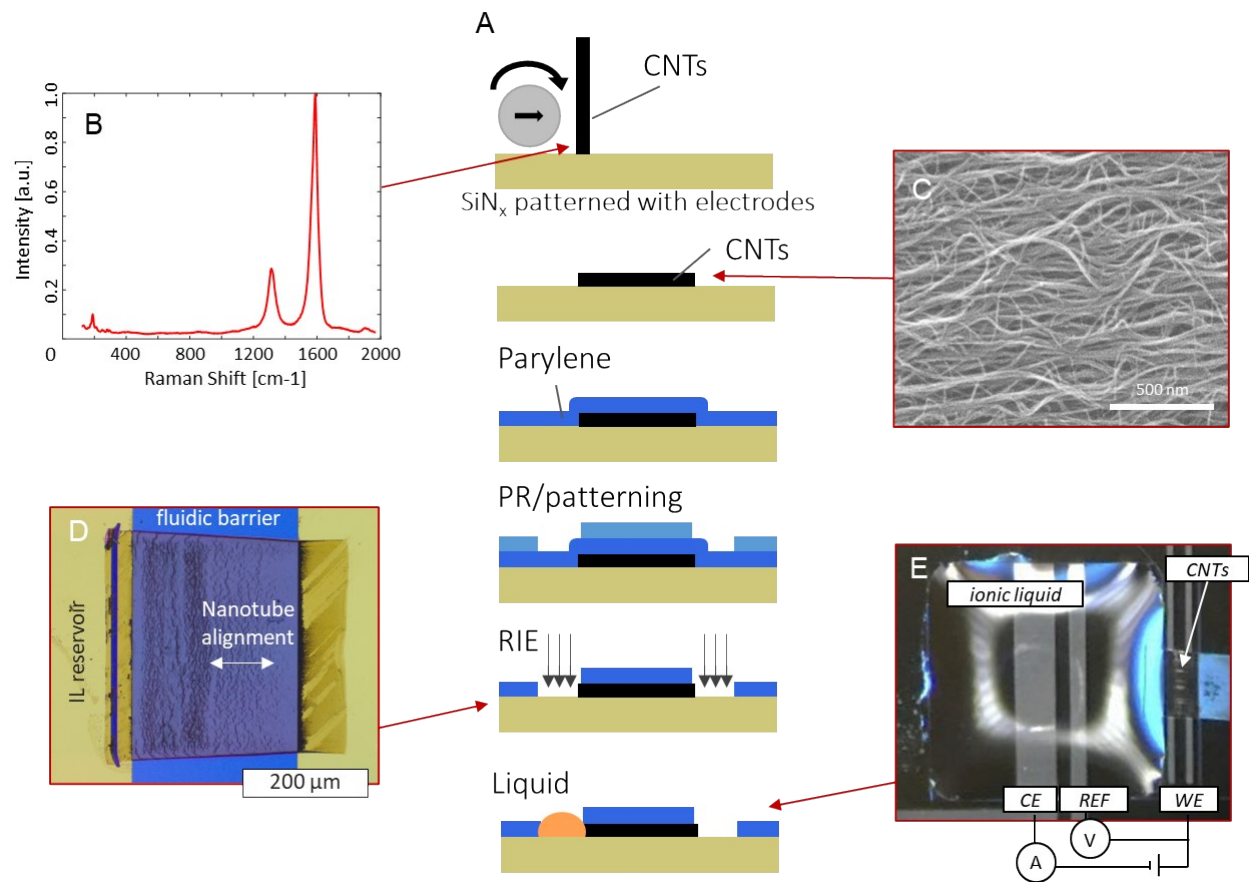


**Figure S4** Schematic showing the fabrication process of our horizontal, electronically and fluidically integrated CNT device. (A) Workflow for device fabrication. (B) Raman spectroscopy of CNTs prior to rolling taken from a device fabricated using catalyst and growth parameters which match those shown in the main text. (C) Electron microscopy image taken from the top down of the CNTs after transition to horizontal state. (D) Optical microscopy image showing parylene infiltrated and tip-etched horizontally aligned CNTs. (E) Optical microscope image showing a drop of IL in contact with one end of the CNTs which sit atop Pt electrodes.

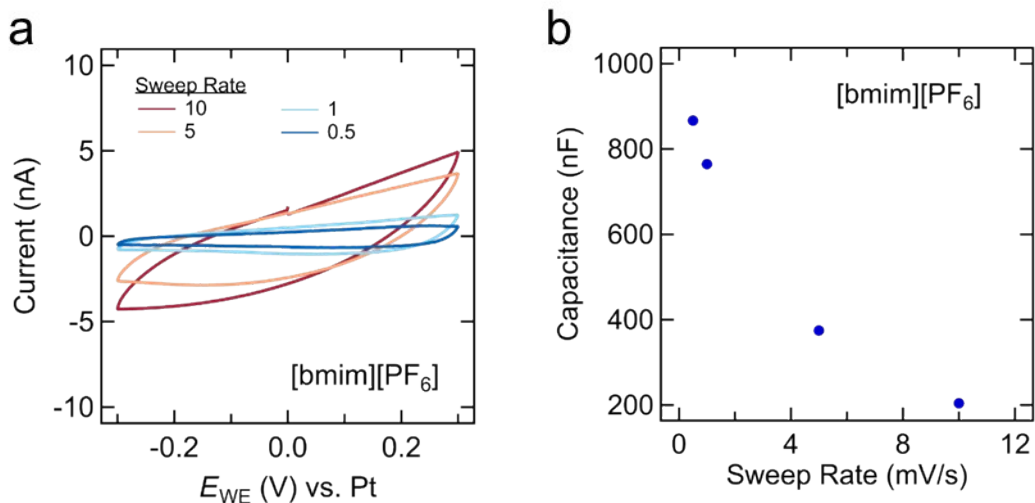


**Figure S5. Cyclic voltammograms of ionic liquid-infilled carbon nanotube electrochemical devices.** (A) Sweep rate-dependent voltammograms of [BMIM][PF<sub>6</sub>] treated devices. (B) Differential capacitance as a function of sweep rate-dependent voltammograms shown in (A). The current was extracted at  $E_{WE} = 0$  V (averaged for forward and reverse scans) and divided by the sweep rate to yield the differential capacitance.

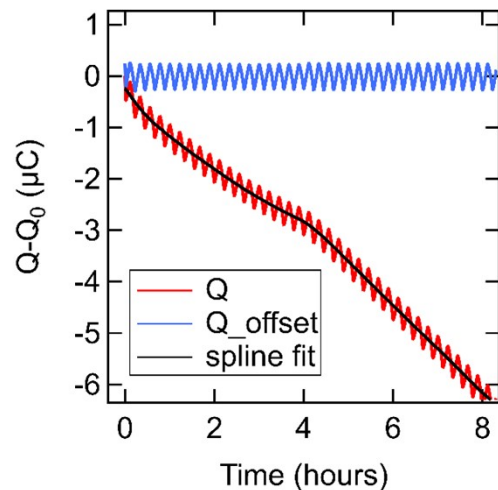


**Figure S6. Method for determining the total capacitance as a function of time.** Cyclic voltammograms were integrated to yield charge ( $Q$ ) vs. time traces (red). These traces consist of an oscillatory charge/discharge component superimposed on a linear decay component. The latter is attributable to some unknown and irreversible electrochemical reaction(s). We eliminate this contribution to the charging current by baseline subtracting a spline fit (black trace) of the charge vs. time trace. The result is the capacitive charge/discharge profile (blue trace). The capacitance is then the maximum charge accumulated for each cycle divided by the voltage range of the voltammogram.

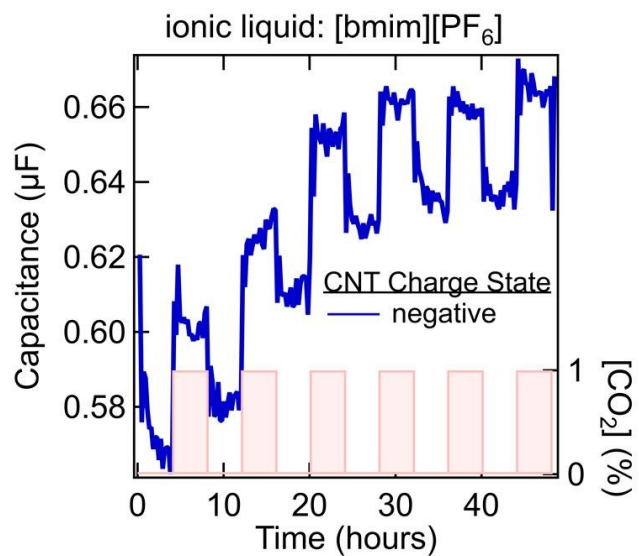


**Figure S7. Repeated exposure to CO<sub>2</sub> gas.** Capacitance vs time for a device which is subjected to 6 consecutive cycles of exposure to 1% CO<sub>2</sub> balanced in N<sub>2</sub> followed by pure N<sub>2</sub>.

## References

1. Kodama, D.; Sato, K.; Watanabe, M.; Sugawara, T.; Makino, T.; Kanakubo, M., Density, Viscosity, and CO<sub>2</sub> Solubility in the Ionic Liquid Mixtures of [bmim][PF<sub>6</sub>] and [bmim][TFSA] at 313.15 K. *Journal of Chemical & Engineering Data* **2018**, *63* (4), 1036-1043.
2. Mondal, A.; Balasubramanian, S., A Refined All-Atom Potential for Imidazolium-Based Room Temperature Ionic Liquids: Acetate, Dicyanamide, and Thiocyanate Anions. *The Journal of Physical Chemistry B* **2015**, *119* (34), 11041-11051.
3. Cabaço, M. I.; Besnard, M.; Danten, Y.; Coutinho, J. A. P., Carbon Dioxide in 1-Butyl-3-methylimidazolium Acetate. I. Unusual Solubility Investigated by Raman Spectroscopy and DFT Calculations. *The Journal of Physical Chemistry A* **2012**, *116* (6), 1605-1620.